
Flow, Turbulence and Combustion **68:** 359–377, 2002.

Organizational Modes of Large-Scale Vortices in an Axisymmetric Turbulent Jet

AMIT AGRAWAL and AJAY K. PRASAD
Department of Mechanical Engineering, University of Delaware, Newark, DE 19716, U.S.A.;
E-mail: {agrawaa,prasad}@me.udel.edu

Received 9 April 2002; accepted in revised form 19 September 2002

Abstract. Large vortices occurring in the axial plane of a self-similar axisymmetric turbulent jet are educed by spatially filtering PIV data. First, the instantaneous PIV frame is convolved with a Gaussian kernel to obtain a smooth (low-pass) field. Next, the low-pass field is Galilean transformed to expose the large vortices residing near the edges of the jet. Large vortices tend to organize themselves in preferred modes; evidence of ring and helical modes is revealed by Galilean transformation of the low-pass filtered field. Both modes seem to occur prominently in jets, with the helical mode being the more frequent. The overall diameter of both ring and helical modes is comparable with the local jet width. The low-pass field occasionally exhibits arrowhead shaped structures with large entrainment at their downstream tips. Stochastic estimates computed from the Galilean-transformed low-pass filtered field indicate that jet meander and a sweep-in of ambient fluid are sufficient to reconstruct large vortices. The frequency of occurrence of modes agrees with previously quoted results.

Key words: arrowhead structure, Galilean transformation, linear stochastic estimate, low-pass filter, PIV, ring and helical modes.

1. Introduction

The ubiquitous presence of coherent structures in turbulent flows was realized after visualization studies in planar mixing layers by Brown and Roshko [6]. Since then, coherent structures have been a subject of great interest in fluid mechanics. It has been established that they affect important practical processes such as dispersion and mixing of fluids in turbulent flows, noise production in the exhaust of an aircraft, and combustion. It is believed that understanding them, and their interaction with themselves and the surrounding fluid will provide new insights into the flow physics.

Although coherent structures in mixing layers are quite well documented, the nature of coherent structures in turbulent jets is not fully established. It is partly because the energy content of coherent motion in jets is lower (about 10%) compared to 20% for mixing layers [9] that makes recognition of structures more difficult in jets. Extensive measurements in the far-field of jets along with better eduction methods are therefore warranted.

Earlier researchers primarily focused on regions close to the jet orifice, and therefore the near-field is well understood. As the jet fluid exits the orifice, a laminar shear layer is formed, which being unstable forms ring vortices. Adjacent vortices pair off, followed by a circumferential instability causing vortex break-up [11]. The jet becomes fully turbulent within about 40 diameters from the orifice, and it was believed that the spatial scales reduce as the vortex rings break up and are convected downstream. However, the correlation measurements with hot-wires by Tso et al. [18], and the high-resolution LIF visualization of low Reynolds number (650–2500) jets by Dimotakis et al. [8] provided evidence of vortices in the far-field of jets whose size was comparable to the local jet width. These led to further investigations to identify coherent structures (and their organization) in turbulent jets. For example, Mungal and Hollingsworth [13] provided evidence of large, coherent vortices in very high Re (2×10^8) jets indicating that large-scale organization is an integral part of jet flows.

Dimotakis et al. [8] found evidence of both axisymmetric and helical modes, and proposed that the far-field of jets was an expanding spiral. Dahm and Dimotakis [7] employed LIF visualization in the far-field of an axisymmetric turbulent jet and concluded the presence of ring and helical modes, with the jet perpetually switching between them. The instantaneous concentration field was ordered in the form of arrowhead-shaped structures, with marginal variation of concentration within these structures. Based on three-dimensional concentration measurements, Yoda et al. [20] proposed that the helical mode exists in pairs, such that a clockwise and a counter-clockwise rotating spiral exist simultaneously. Further, they provided evidence of structures with a conical downstream end. Siddhartha et al. [16] also reported arrowhead-shaped structures which telescope negligibly into their downstream counterparts from their numerical simulations.

Tso and Hussain [17] conducted measurements in jets with a rake of X-wires and concluded that the helical mode is the most preferred and occurs 12% of the time. The double helical mode was found to occur 3% of the time. The ring mode, although present, was not considered to be dynamically important in the jet far-field. On the other hand, Yoda et al. [19] found organizational modes for almost *all* their realizations. They also found that helical and ring modes occur with almost equal probability, and that the structures maintain themselves for a large downstream distance. Although it appears at first glance that the frequency of modes seen by Yoda et al. [19] is far greater than that observed by Tso and Hussain [17], we will subsequently show that their results are actually in close agreement with each other, and with our results as well. Tso et al. [18] suggested that these structures persist for about three times the local jet width.

Interestingly, even before the presence of ring and helical modes in axisymmetric jets was experimentally confirmed, they had been predicted by several theoretical studies. For example, linear stability analysis of inviscid jets by Batchelor and Gill [5] showed that only the helical mode can produce amplified disturbances.

Similarly, the linear stability analysis of Michalke [12] had suggested that the helical mode is the most unstable mode.

Experimental studies to date differ in their descriptions of these organizational modes perhaps due to the difficulty involved in identifying coherent structures. Tools employed by previous researchers – visualization methods, and conditional averaging of pointwise data – have limitations in exposing a vortex: visualization methods cannot provide quantitative information, and pointwise measurements suffer from inadequate spatial resolution. Therefore, neither is ideally suited for such investigations. Both of these difficulties, however, are surmounted by whole field velocimetry techniques such as PIV.

PIV allow simultaneous velocity measurements at a large number of points over extended planar domains. A low-pass filtering operation on the PIV velocity data exposes the largest structures (and removes the smaller vortices from the flow field). The streamline pattern for the educed vortex in the low-pass field is closed for a large radial extent making the identification process robust. A detailed description of the low- (and high-) pass filtering technique is presented in [2, 3]. An additional advantage of whole field velocimetry is that along with quantitative information of a vortex, the velocity of the neighboring fluid is also available. For example, induced velocities in the surrounding field due to the Biot–Savart effect of coherent structures can also be deduced from PIV data. Therefore, PIV coupled with the low-pass filtering technique constitutes an effective tool to study the organizational modes in a jet.

This paper focuses on results from the low-pass filtered field. Vortices occurring in the high-pass field have been discussed earlier [3, 4]. Briefly, Agrawal and Prasad [3] present results for pdf's of vortex circulation, energy and frequency of occurrence as a function of the radial coordinate in jets. In [4] the focus is on the radial distribution of circulation and other properties *within* vortex cores. High-pass results from [3, 4] will be contrasted in the following sections with the low-pass field results which form the thrust of the current paper.

In this work, we examine the organizational modes of the larger vortices educed from the low-pass filtered velocity data in the axial plane of a turbulent axisymmetric jet. Our goal is to characterize these modes in an unambiguous and quantitative manner. Organizational modes of the larger vortices are revealed by a suitable Galilean transformation of the low-pass filtered field. Stochastic estimates are computed to estimate the frequency of occurrence of the organizational modes and to understand the mechanisms responsible for the production of the larger vortices.

2. Experimental Setup

PIV measurements were conducted in a 1.2 m tall glass tank with a 0.5 m square cross-section, which houses a nozzle at the bottom (orifice diameter, $d = 2$ mm). The jet was directed upwards and measurements were conducted in an axial plane (x, z) of the jet. Twin Nd-YAG pulsed lasers (350 mJ/pulse at 532 nm) provided

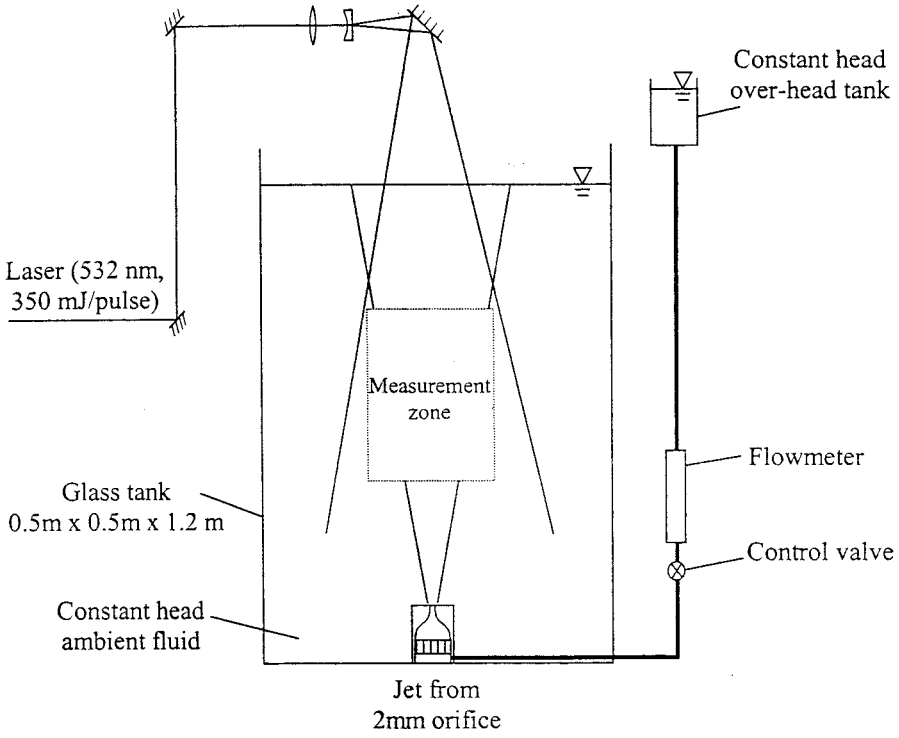

Figure 1. Experimental set-up.

illumination for PIV with a pulse separation of 12 ms (Figure 1). 8 μm hollow spherical glass particles were used as tracers for PIV with water as the working fluid. Images were recorded using a Kodak 1.0 ES camera with a 1026×1000 pixels array. Frames were captured at 0.5 Hz such that successive frames were statistically uncorrelated. Measurements were conducted for a jet Reynolds number, Re (based on d and the exit velocity) of 3000. A small magnification (1/13) was employed to ensure that an adequate jet width was captured in the viewframe. The viewframe ($110 \leq z/d \leq 175$) containing 60×60 vectors was centered on the jet axis.

The definition of Robinson et al. [15]: "A vortex exists when instantaneous streamlines mapped on to a plane normal to the core exhibit a roughly circular or spiral pattern, when viewed in a reference frame moving with the center of the vortex core", is used here for the definition of a vortex. The rotational sense of vortices is obtained in the conventional way, i.e., positive if the center of the eddy is to the left while transversing the path, and negative otherwise.

3. Techniques Employed

A few specialized data processing methods have been employed in this work. A brief overview of these techniques is provided here; additional details may be found in [3].

3.1. Low-pass filtering

PIV data is spatially filtered to educe the vortical structures in the flow field. Filtering is achieved by convolving the instantaneous velocity field by a Gaussian kernel. The convolution operation produces a smooth (low-pass filtered) field by suppressing the higher frequency content. The lowest retained frequencies correspond to the largest vortices in the flow. The standard deviation of the smoothing Gaussian kernel was set to three grid units, and the filter was truncated at five grid units. The choice of the smoothing parameters was dictated solely by the constraints imposed during the eduction of the small vortices in the high-pass filtered field [3]. These parameters were chosen after a careful iterative process to ensure that the high-pass filtered field reproduced all the vortices that could also be exposed by Galilean transformation. On the other hand, the large vortices in the low-pass filtered field are far less sensitive to the choice of the parameters. Consequently, we have retained the original values for the sake of continuity. In fact, using the same values of parameters in [3] and in the current paper ensures that the entire spectrum of vortices is educed with minimal adjustment of user-supplied parameters. Further, the chosen parameters educe vortices only on the order of the jet width (i.e., vortices of diameter larger than 11 grid units) in the low-pass filtered field.

3.2. Galilean transformation

Galilean transformation involves a simple change of the reference frame. It is performed by subtracting a constant velocity from the entire velocity field [2, 3]. Vortices with an advection velocity close to the subtracted velocity are exposed by this process. Successive Galilean transformations with a gradual increment of the subtracted velocity can educe all the resolvable vortices from an instantaneous PIV realization.

3.3. Linear stochastic estimation

Stochastic estimation is a useful tool to reconstruct a velocity field conditioned upon one or more events, from a set of whole-field velocity data [1, 10, 14]. A large data-set of instantaneous PIV vector fields collected under identical conditions, and one (or more) event vector(s) are the inputs to this technique. A large data-set is critical for success, whereas the number of specified events should be kept to a minimum. The output (estimated field) is obtained by minimizing the

root-mean-square error between the estimated and the instantaneous input fields. The technique has been successfully employed to educe both the dominant and the underlying structures in stationary turbulent flows. For example, Prasad and Gonuguntla [14] applied it to high-Rayleigh number turbulent thermal convection and obtained insight into the various modes in their flow.

Stochastic estimation of PIV data is somewhat equivalent to conditional averaging of pointwise data. For both of these techniques, an event vector is specified and a vector field surrounding the event vector is obtained. The primary difference is that the former constitutes a least-squares fit to the *entire* data-set, whereas the latter averages *only* that subset of the data which contains the specified event vector. It should be noted that due to its least-squares nature, a stochastic estimate need not resemble any of the instantaneous data-fields that serve as the input.

Mathematical details of this technique presented here are adapted from [1, 14]. Let $u_i(\boldsymbol{x}')$ represent all of the available data. If the specified event vector is $u_j(\boldsymbol{x})$, and the vector field predicted by stochastic estimation is $\hat{u}_i(\boldsymbol{x}')$, then we may write:

$$\hat{u}_i(\boldsymbol{x}') = A_{ij}(\boldsymbol{x}', \boldsymbol{x}) u_j(\boldsymbol{x}),$$

where $A_{ij}(\boldsymbol{x}', \boldsymbol{x})$ is the coefficient matrix. The mean square difference between the estimated field and the data needs to be minimized, i.e.,

$$\left\langle [u_i(\boldsymbol{x}') - \hat{u}_i(\boldsymbol{x}')]^2 \right\rangle = \left\langle [u_i(\boldsymbol{x}') - A_{ij}(\boldsymbol{x}', \boldsymbol{x}) u_j(\boldsymbol{x})]^2 \right\rangle = \text{minimum}.$$

Upon applying the orthogonality principle for minimization which states that the errors $[u_i(\boldsymbol{x}') - A_{ij}(\boldsymbol{x}', \boldsymbol{x}) u_j(\boldsymbol{x})]$ are statistically orthogonal to the data, we obtain the following necessary condition:

$$\left\langle [u_i(\boldsymbol{x}') - A_{ij}(\boldsymbol{x}', \boldsymbol{x}) u_j(\boldsymbol{x})] u_k(\boldsymbol{x}) \right\rangle = 0.$$

A_{ij} is then determined by using the two-point correlations according to:

$$A_{ij}(\boldsymbol{x}', \boldsymbol{x}) = \left\langle u_i(\boldsymbol{x}') u_k(\boldsymbol{x}) \right\rangle \left\langle u_j(\boldsymbol{x}) u_k(\boldsymbol{x}) \right\rangle^{-1}.$$

Finally,

$$\hat{u}_i(\boldsymbol{x}') = \left\langle u_i(\boldsymbol{x}') u_k(\boldsymbol{x}) \right\rangle \left\langle u_j(\boldsymbol{x}) u_k(\boldsymbol{x}) \right\rangle^{-1} u_j(\boldsymbol{x}). \tag{1}$$

The estimated field $\hat{u}_i(\boldsymbol{x}')$ is such that its mean square error with respect to the measured data has been minimized. It is the best mean square estimate.

If the specified event is a single-point event, $\langle u_j u_k \rangle$ is a 2×2 matrix:

$$\langle u_j u_k \rangle = \begin{bmatrix} \langle u_1 u_1 \rangle & \langle u_1 u_2 \rangle \\ \langle u_2 u_1 \rangle & \langle u_2 u_2 \rangle \end{bmatrix}$$

where $u_1 = u$ and $u_2 = w$. If a two-point event is specified, $\langle u_j u_k \rangle$ is a 4×4 matrix:

$$\langle u_j u_k \rangle = \begin{bmatrix} \langle u_1^1 u_1^1 \rangle & \langle u_1^1 u_2^1 \rangle & \langle u_1^1 u_1^2 \rangle & \langle u_1^1 u_2^2 \rangle \\ \langle u_2^1 u_1^1 \rangle & \langle u_2^1 u_2^1 \rangle & \langle u_2^1 u_1^2 \rangle & \langle u_2^1 u_2^2 \rangle \\ \langle u_1^2 u_1^1 \rangle & \langle u_1^2 u_2^1 \rangle & \langle u_1^2 u_1^2 \rangle & \langle u_1^2 u_2^2 \rangle \\ \langle u_2^2 u_1^1 \rangle & \langle u_2^2 u_2^1 \rangle & \langle u_2^2 u_1^2 \rangle & \langle u_2^2 u_2^2 \rangle \end{bmatrix}.$$

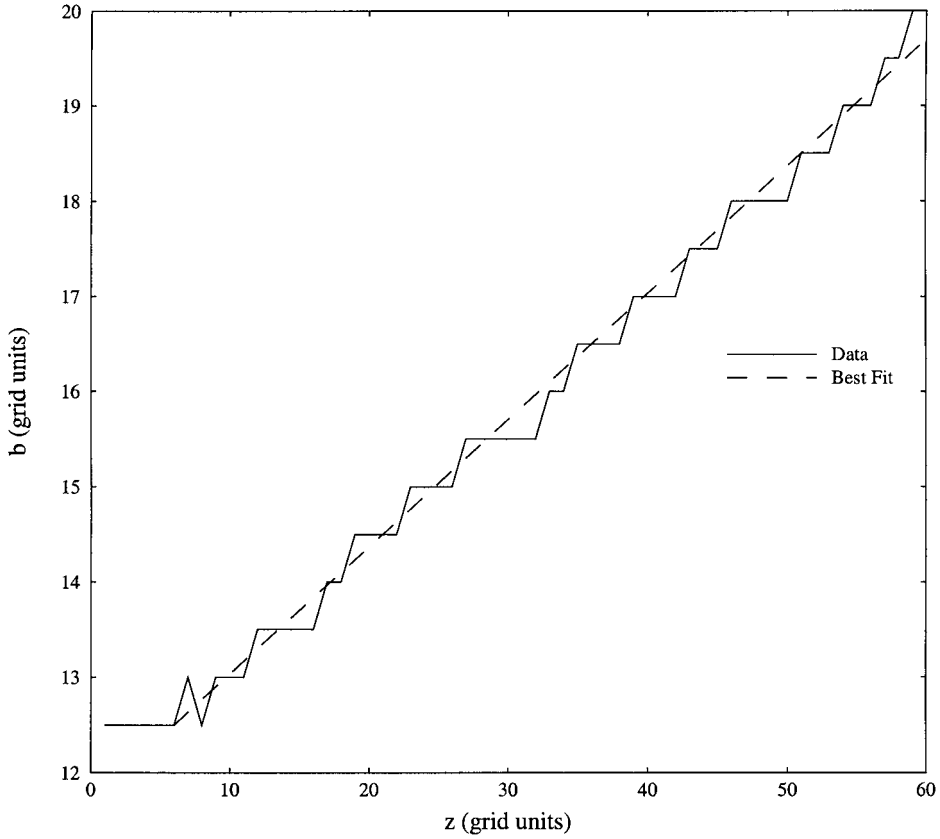

Figure 2. Axial variation of the jet width.

For a two-point event, superscripts 1 and 2 refer to the first and second points respectively.

Terms like $\langle u_1 u_2 \rangle$ denote two-point correlations, which were computed using the entire data set according to:

$$\langle u_1 u_2 \rangle = R_{u_1 u_2}(x, z, x', z') = \frac{1}{N} \sum_{1}^{N} u_1(x, z) u_2(x', z'), \tag{2}$$

where (x, z) and (x', z') represent the first and second point in the two-point correlation respectively, and N is the total number of realizations in the ensemble (222 in our case).

4. Results and Discussion

Results presented in this paper pertain to a jet Reynolds number of 3000, with the viewframe located between $110 \leq z/d \leq 175$. The jet width, b (defined as

the radial location at which the mean streamwise velocity reduces to e^{-1} of the mean centerline velocity) varies linearly with the downstream coordinate, z. For the present configuration b varies between 12 and 20 grid units ($\sim$ 24–40 mm) from bottom to top of the viewframe (Figure 2). The growth rate of the jet ($\mathrm{d}b/\mathrm{d}z = 0.11$) agrees with published data. Each PIV frame contains 60×60 vectors on a square grid, and therefore contains a minimum of $1.5b$ on either side of the jet axis, and about four times the nominal jet width along z. The Kolmogorov length scale for the present configuration is approximately 0.2 mm. Our data set consists of 222 statistically independent frames.

4.1. Examination of the largest vortices from low-pass filtered data

The largest structures are educed by means of Galilean transformation, i.e., by subtracting the advection velocity of the vortices (about 15% of the nominal centerline velocity) from the low-pass filtered fields. (The nominal centerline velocity refers to the centerline velocity at the center of the view frame.) As noted earlier, only vortices larger than the cut-off filter size ($R > 5$ grid units) are exposed in the low-pass filtered field. These largest vortices are rather infrequent (average of three per frame) and are generally located near the jet boundaries. (Note that the operations of Galilean transformation and low-pass filtering are commutative. Therefore the results are independent of the order in which these are performed.) Our intention was to inspect the resulting field for any preferred arrangement of the largest vortices, i.e., does the low-pass Galilean transformed field provide evidence for the previously observed ring or helical modes?

Examination of individual PIV realizations revealed that about one in three frames indicates the presence of such modes. In other words, modes are present 1/3 of the time over a downstream distance equal to four times the jet width at the center of the frame. We estimate the viewfield ($30 \leq z/d \leq 83$) of Yoda et al. [19] as 10 times the jet width at the center of their frame. Assuming that the probability of mode occurrence correlates with the size of the viewfield, Yoda et al. [19] should discern modes 2.5 times more frequently than us. Our result is therefore consistent with their [19] observation that modes are almost always present. Tso and Hussain's [17] apparently infrequent observation of modes (15%) can also be explained in a consistent manner. They made their measurements with a rake of X-wires spanning 1.5 times the jet width, therefore their equivalent "viewframe" would correspond to a downstream distance of $1.5b$. Assuming that a viewframe that is $10b$ long in the axial direction will almost always exhibit a mode [19], Tso and Hussain's [17] frequency of mode detection should then correspond to $1.5/10 = 15\%$.

We will first provide evidence of the organizational modes from individual Galilean-transformed PIV realizations. Figure 3 shows two vortices centered at (5, 30) and (56, 30) rotating CCW and CW respectively. The size and shape of the

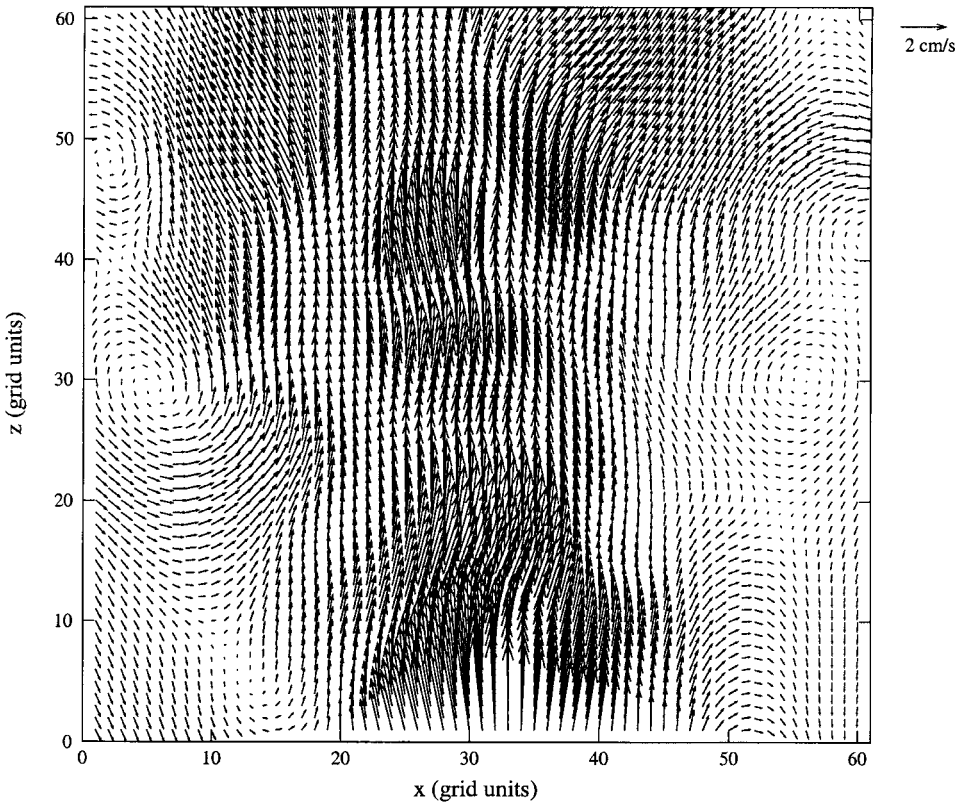

Figure 3. Ring mode obtained by Galilean transformation of low-pass filtered field ($110 \leq z/d \leq 175$, 1 grid unit = 2 mm).

vortices are comparable indicating that they might belong to the same axisymmetric ring (of radius 25.5 grid units). Another pair of rings (truncated by the edge of the frame) with a slightly larger radius can also be discerned in the frame at $z \approx 45$.

Figure 4 shows four vortices: those centered at (10, 5) and (10, 31) rotate CCW, while those at (52, 16) and (51, 49) rotate CW. While the horizontal separation between the eddies remains roughly constant (42 grid units), the vertical separation between successive vortices (of 11, 15, 18 grid units respectively) increases downstream. These four vortices could jointly represent an expanding helical structure residing near the edge of the jet. The inner core of the jet in Figure 4 appears to contain arrowhead-shaped structures.

A better example (without Galilean transformation) containing three arrowhead-shaped structures is presented in Figure 5. Note the uniformity in vector size within each structure, indicating little variation in velocity within it. This observation is consistent with the concentration measurements of Dahm and Dimotakis [7]. In addition, large inward velocities occur at the downstream end of the upper-most structure. This indicates that these arrowhead shaped structures induce entrainment

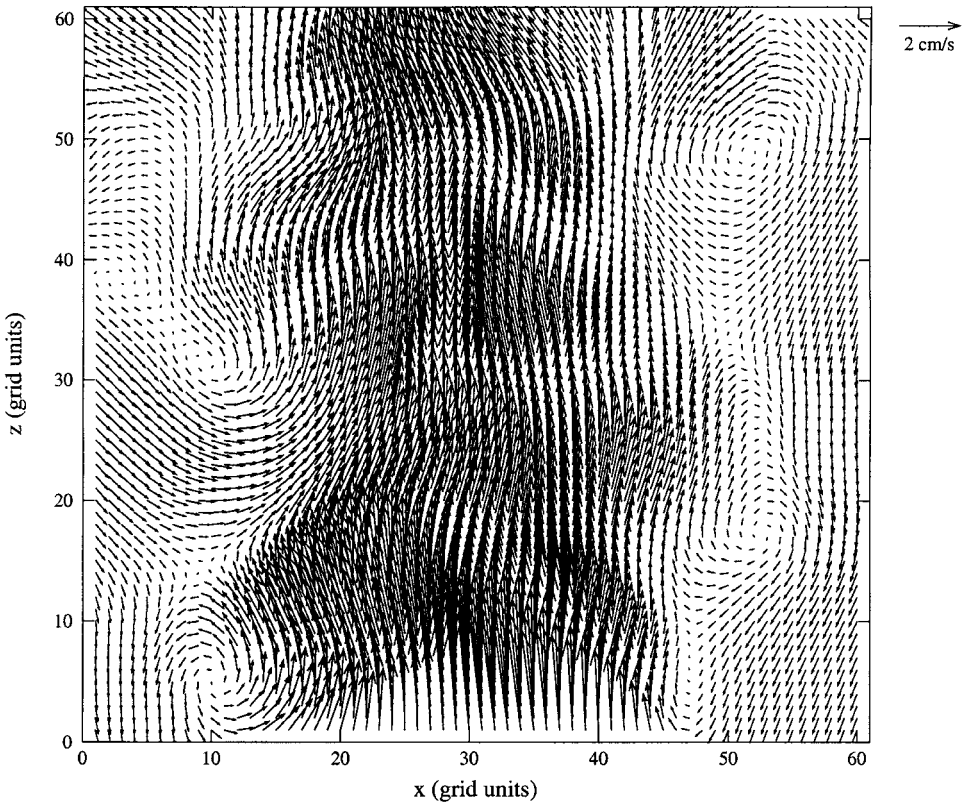

Figure 4. Helical mode obtained by Galilean transformation of low-pass filtered field ($110 \leq z/d \leq 175$, 1 grid unit = 2 mm).

near their tips, or, conversely, large entrainment causes the conical shape of these structures. A similar observation has been reported by Yoda et al. [19]. One might expect a ring mode at the (somewhat symmetric) base of the structure, however our data set does not provide evidence for it (see Figure 4).

Agrawal and Prasad [3] found that substantial numbers of smaller vortices in the high-pass field can have a rotational sense opposite to that suggested by the time-averaged vorticity value. In other words, they found a sizable fraction of vortices rotating CCW (CW) in the right (left) half-plane of the jet. However, Figures 3 and 4 show that the largest vortices always rotate CW in the right half-plane and CCW in the left half-plane, i.e., their rotational sense correlates with the time-averaged vorticity value. This observation is consistent with the idea of engulfing vortices residing at the edges of the jets proposed by Dimotakis et al. [8]. The large vortices induce a Biot–Savart velocity in the ambient irrotational fluid. The ambient fluid is subsequently ingested into the body of the jet, and finally, by straining and molecular diffusion, mixes thoroughly into the jet fluid.

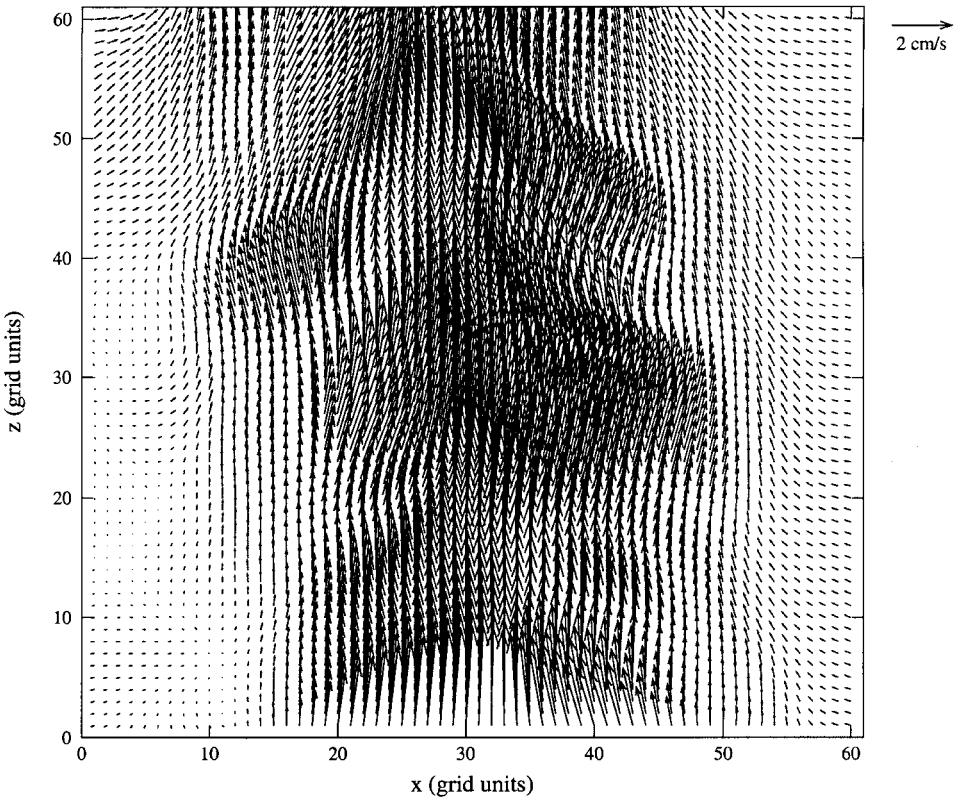

Figure 5. Arrowhead shaped structures from low-pass filtered field ($110 \leq z/d \leq 175$, 1 grid unit = 2 mm).

4.2. EDUCTION OF MODES BY STOCHASTIC ESTIMATION

As seen above, Galilean transformation of the low-pass filtered field reveals the largest vortices present in the frame. Stochastic estimation was then applied to investigate the robustness of these organizational modes. Stochastic estimates were computed for one- and two-point event vectors (two and four events respectively). Stochastic estimation proceeds in the following manner:

1. The instantaneous PIV frame is low-pass filtered.
2. The low-pass field is Galilean transformed by subtracting about 15% of the ensemble-averaged centerline velocity at the center (along z) of the frame. As seen above, this is approximately the advection velocity of the structures, and therefore educes the vortices. (Results are not very sensitive to the amount subtracted for Galilean transformation. For example, almost identical stochastic estimates are obtained for 15 and 20%.)
3. Two-point correlations are computed according to Equation (2) and stored.

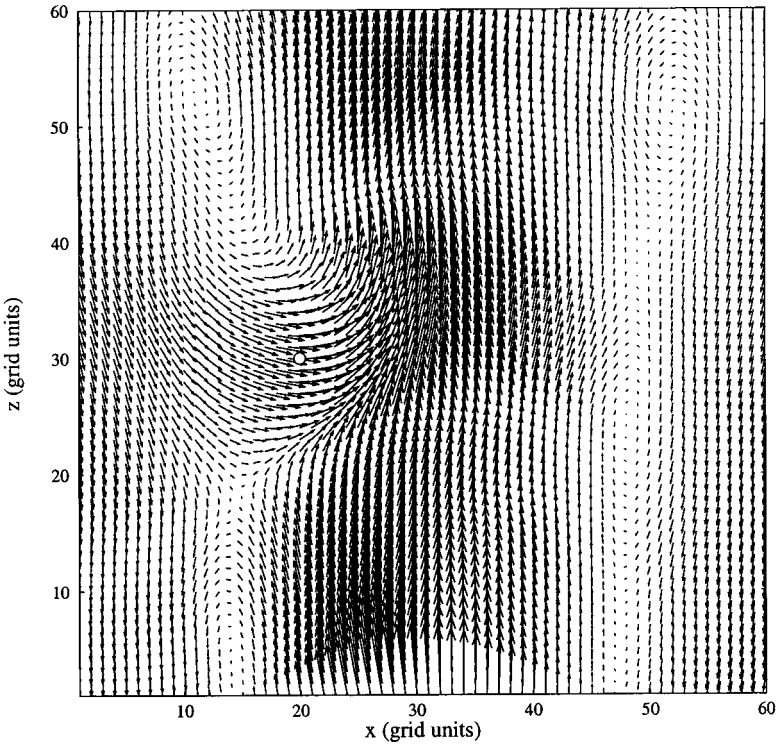

Figure 6. Single-point stochastic estimate showing a ring mode; event $(1, 0)$ specified at $(20, 30)$ corresponds to a sweep-in of ambient fluid. (The open circle specifies the location of the event-vector. $110 \leq z/d \leq 175$, 1 grid unit = 2 mm.)

4. Event vectors are specified at the chosen point(s). The choice of the event vector and its location is decided after several careful iterations and the most illustrative examples are presented here. Values of the specified events u_{event} and w_{event} are hereby represented as $(u_{\text{event}}, w_{\text{event}})$. Note that, if u_{event} and w_{event} are multiplied by a constant, the stochastic estimated field also scales by that constant (and remains qualitatively unchanged). We therefore set either u_{event} or w_{event} to unity.
5. The stochastic estimate is computed according to Equation (1).

It should be noted that the chosen event vector should agree within machine precision with the corresponding vector calculated by the stochastic estimation program. This important check was successfully performed for all the results presented here.

First, results are presented for a single-point event vector, and then for a two-point event vector.

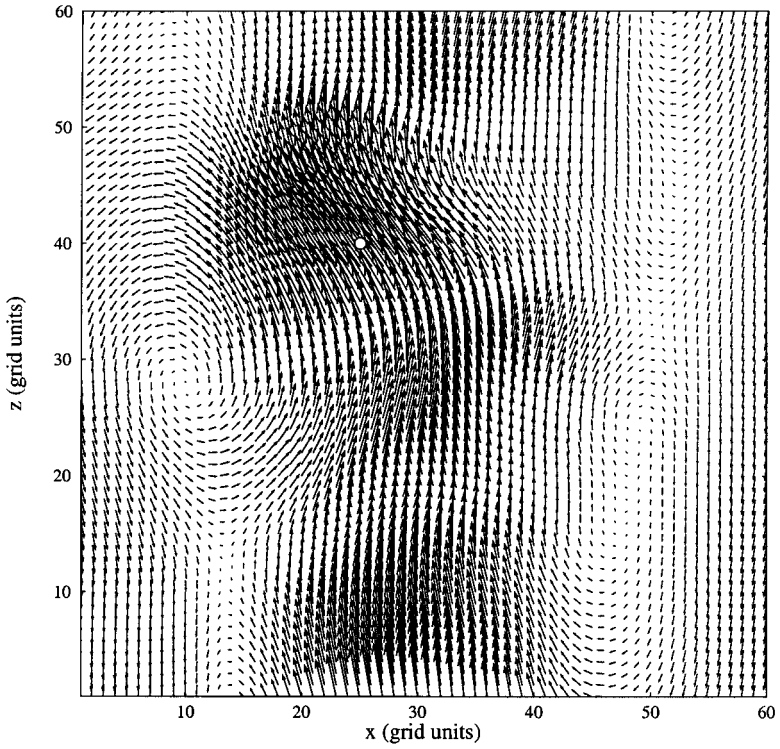

Figure 7. Single-point stochastic estimate showing a ring mode; event $(-0.7, 1)$ specified at $(25, 40)$ corresponds to jet meander. Note the jet tilt is exaggerated because of Galilean transformation. ($110 \leq z/d \leq 175$, 1 grid unit = 2 mm.)

4.2.1. *Single-Point Event Estimates*

A ring mode appears if a large inward sweep of ambient fluid into the jet is specified at either side (Figure 6), or if the jet is forced to meander to one side (Figure 7). Here, "inward sweep" refers to the situation in which the velocity of the neighboring (ambient) fluid is directed toward the jet-axis. "Jet meander" refers to a situation where the fluid at the jet centerline bends either to the left or the right. In Figure 6, the event vector $(1, 0)$ located towards the left edge at $(20, 30)$ ensured an inward sweep of the ambient fluid (note that the stochastic estimate necessarily produces highly smooth vector fields, and therefore this event will induce a substantial portion of fluid in its neighborhood to be directed towards the centerline). The specified event led to the emergence of ring-mode vortices at $(11, 53)$ and $(52, 51)$. (Large shear at the edges of the jet seems to be responsible for the distortion of vortices.) In Figure 7, a leftward meander forced by the event vector $(-0.7, 1)$ specified slightly away from the centerline at $(25, 40)$ spawned vortices centered at $(10, 28)$ and $(49, 24)$. Although the event vector represents a strong tilt away from the vertical, the severity of the tilt is somewhat exaggerated as the

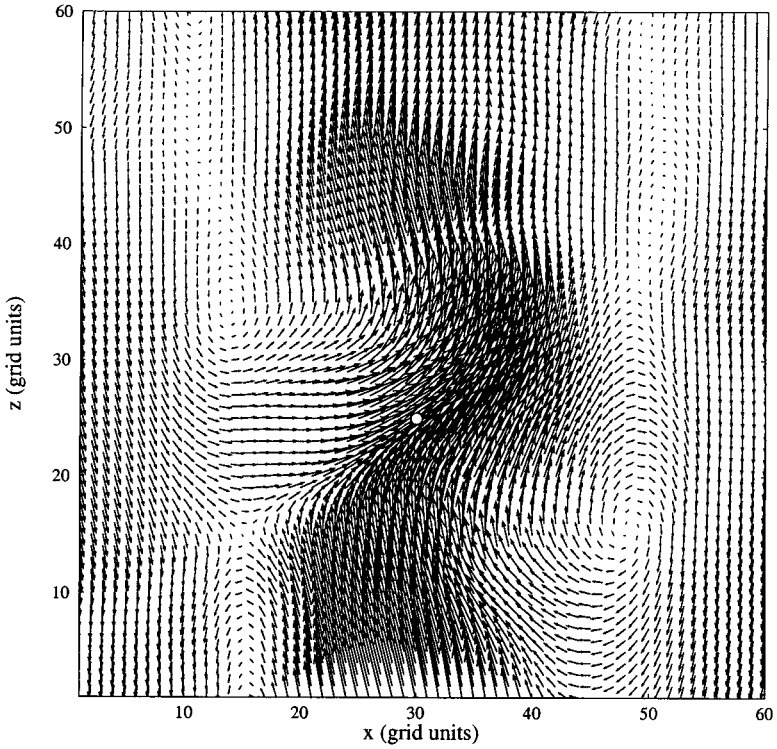

Figure 8. Single-point stochastic estimate showing a helical mode; event (1, 1) specified at (30, 25) corresponds to jet meander. Note the jet tilt is exaggerated because of Galilean transformation. ($110 \leq z/d \leq 175$, 1 grid unit = 2 mm.)

input fields are Galilean transformed by subtracting 15% of the nominal centerline velocity. Note that the radius of the emerging vortex ring is about 20 grid units (Figures 6 and 7), and is comparable to the local jet width (Figure 2).

Figure 8 shows another stochastic estimate field obtained by forcing the jet to the right with an event (1, 1) located at the centerline (30, 25) leading to the emergence of vortices centered at (49, 15), (15, 35) and (51, 45) while a fourth vortex might be present at the base of the frame. These vortices could belong to a helical coil (radius of about 17 grid units) encircling the jet.

4.2.2. *Two-Point Event Estimates*

These results are obtained by specifying a total of four events. The first result in Figure 9 pertains to event vectors (0.7, 1) located at (29, 10), and (0.7, 1) at (30, 60) respectively, i.e., an in-phase meander is forced on the jet. A ring structure near the top of the frame with centers at (8, 51) and (52, 48) appears, while a second ring structure centered at (46, 5) and (13, 17) can also be discerned. These rings are clearly defined and can therefore be more easily discerned than the corresponding rings in Figures 6 and 7. This and subsequent results indicate the benefit

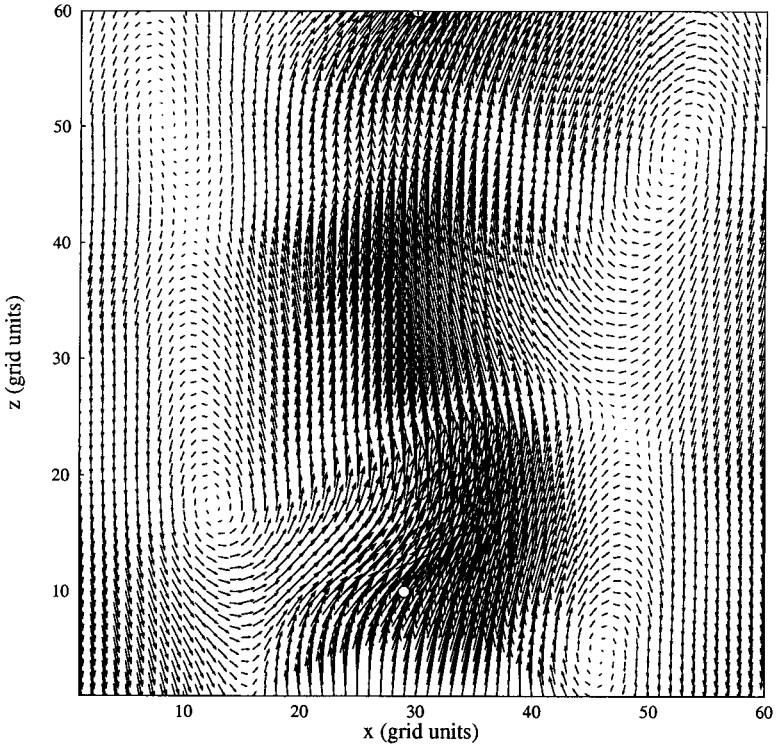

Figure 9. Two-point stochastic estimate showing a ring mode: (0.7,1) specified at (29, 10), and (0.7, 1) specified at (30, 60). Note the jet tilt is exaggerated because of Galilean transformation. ($110 \leq z/d \leq 175$, 1 grid unit = 2 mm.)

of computing stochastic estimates based on four events. Two interesting observations about these vortex rings can be made. First, the right vortex somewhat trails its left counterpart. In other words, the axis of the vortex ring does not coincide with the time-averaged jet axis, rather it is aligned with the local instantaneous centerline velocity vector. Second, the radial location of the two vortex rings (22 and 16.5 grid units respectively) are roughly equal to the local jet widths. Both these facts, support our conclusion that the vortices indeed belong to the same vortex ring.

It was observed that upon specifying event vectors at two points, the helical mode is more easily reconstructed than the ring mode. In Figure 10, both the event vectors are located away from the axis at (15, 2) and (48, 23). The specified events, (1, 0) and (−0.4, 0) respectively, provide inward sweeps of ambient fluid. The specified events are probably individually responsible for the proximal vortices at (12, 13) and (52, 33), while they jointly spawn the vortex at (9, 53). These vortices appear to be part of a helical coil of approximate radius 21 grid units.

A final example is provided in Figure 11, where four vortices centered at (8, 17), (53, 24), (6, 43) and (59, 54) are exposed by specifying the event vector (0.4, 0)

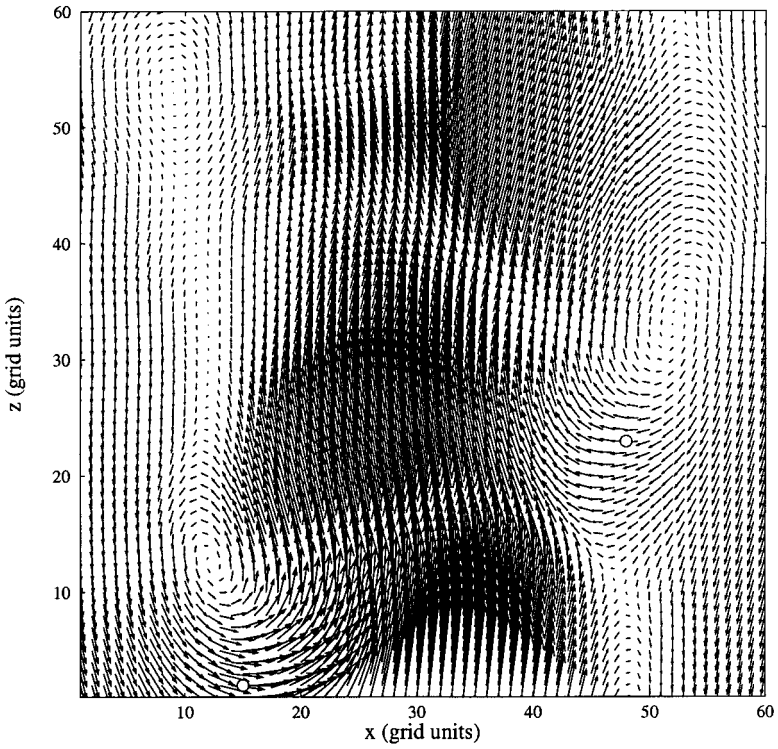

Figure 10. Two-point stochastic estimate showing a helical mode: (1, 0) specified at (15, 2), and (−0.4, 0) specified at (48, 23). ($110 \leq z/d \leq 175$, 1 grid unit = 2 mm.)

at (10, 10), and (−0.4, 1) at (50, 50) respectively. Both event vectors ensure an inward sweep of ambient fluid, and are individually responsible for the corresponding proximal vortex. While the two vortices on the left plane rotate CCW, those on the right rotate CW. The four vortices belong to a single helical coil around the jet at its boundary. Note the arrowhead shaped underlying structures. The large inward velocity at the tips of the arrowhead is evident, and replicates the instantaneous observations.

Note that when specifying four events, a significant tilting of the jet is no longer essential (compare Figures 10 and 11 to Figures 6–8). Stochastic estimates based on two-point events appear to be more physically intuitive than single-point events, owing perhaps to the fact that velocities in a turbulent jet become weakly correlated as the downstream separation increases.

It should be noted that specifying events with a magnitude or direction slightly different than those reported in the paper resulted in a similar looking structure at almost the same location. As stated before, event vectors and their locations were chosen such that the most illustrative flow fields are extracted. Further, the event vector should be specified with some care such that only physically realistic fields are constructed.

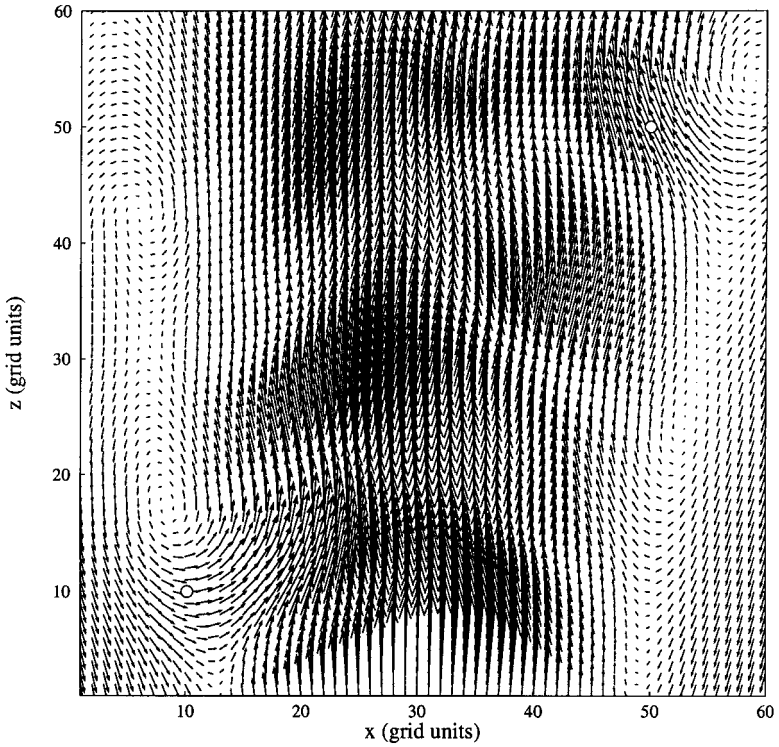

Figure 11. Two-point stochastic estimate showing a helical mode: (0.4, 0) specified at (10, 10), and (−0.4, 1) specified at (50, 50). Note the underlying arrowhead shaped structures. ($110 \leq z/d \leq 175$, 1 grid unit = 2 mm.)

It is evident from the examples cited above that a large inward sweep of the ambient fluid, and jet meander are primarily associated with the appearance of vortices. These judgements were made in the post-processing, i.e., upon examining the ensuing vector field. Several alternative event combinations were attempted; for example, we tried to educe vortices by specifying up and down event-vectors at the same z location but separated by a small x, or, left and right event-vectors at the same x and separated in z. These combinations however did not educe any mode. They did produce a vortex on one side of the jet axis, however the corresponding pair on the other side of the jet-axis could be hardly discerned.

5. Conclusions

Organizational modes of large vortices occurring in the axial plane of a self-similar axisymmetric turbulent jet are examined in this paper. The consistent presence of these modes deduced from the application of Galilean transformation, and one- and two-point stochastic estimation, attests to their robustness for this flow field. The vortices are educed using a two-step process. First, a low-pass filtered field

is obtained by convolving the instantaneous velocity field by a Gaussian kernel. Next, the low-pass field is Galilean transformed to expose the largest vortices. The advection velocity of these vortices is about 15% of the local mean centerline velocity. Ring and helical modes, and arrowhead shaped structures are evident after suitable combination of these operations. Ring and helical modes were found in 1/3 of the total number of acquired frame (the frame covered a downstream length of $4b$). Our result is consistent with Yoda et al. [19] who report that a mode was almost always present over a viewframe of length $10b$, and Tso and Hussai [17] who report that a mode was present 15% of the time over an equivalent viewframe of $1.5b$. The helical mode appears to be more dominant of the two. Perhaps the double helical mode is more difficult to observe, and has not been discerned from our data set.

Analysis of the modes reveals several useful features. The diameter of the educed vortex ring is comparable with the local jet width, and its axis is aligned with the local instantaneous centerline velocity vector. Evidence of two vortex rings occurring simultaneously over a downstream distance of four times the average jet width is provided. The existence of a helical coil comprising up to four vortices is presented. The spacing between adjacent vortices for the helical coil increases with downstream distance, while its diameter is of the order of the local jet width indicating presence of an expanding spiral encompassing the jet body.

The prominent occurrence of ring, helical, and arrowhead structures in the Galilean transformed low-pass filtered field is consistent with their appearance in the fields computed by stochastic estimation. Stochastic estimates revealed that while it is more difficult to reconstruct modes by a single-point event vector, both ring and helical modes can be rather easily exposed by specifying event-vectors at two-points. Further, it indicates that a large entrainment of ambient fluid into the jet body, and jet meander are the primary features associated with the production of large-scale vortices.

Acknowledgement

This work was supported by National Science Foundation, under grant NSF-ATM-9714810.

References

1. Adrian, R.J., Stochastic estimation of conditional structure: a review. *Appl. Sci. Res.* **53** (1994) 291–303.
2. Adrian, R.J., Christensen, K.T., and Liu, Z.-C., Analysis and interpretation of instantaneous turbulent velocity fields. *Exp. Fluids* **29** (2000) 275–290.
3. Agrawal, A. and Prasad, A.K., Properties of vortices in the self-similar turbulent jet. *Exp. Fluids* **33** (2002) 565–577.
4. Agrawal, A., and Prasad, A.K., Measurements within vortex cores in a turbulent jet. *J. Fluids Engrg.* (submitted).

5. Batchelor, G.K. and Gill, A.E., Analysis of the stability of axisymmetric jets. *J. Fluid Mech.* **14** (1962) 529–551.
6. Brown, G.L. and Roshko A., On density effects and large structure in turbulent mixing layers. *J. Fluid Mech.* **64** (1974) 775–816.
7. Dahm, W.J.A. and Dimotakis, P.E., Mixing in large Schmidt number in the self-similar far field of turbulent jets. *Phys. Fluids* **217** (1990) 299–330.
8. Dimotakis, P.E., Maike-Lye, R.C. and Papantoniou, D.A., Structure and dynamics of round turbulent jets. *Phys. Fluids* **26** (1983) 3185–3192.
9. Fiedler, H.E., Coherent structures. In: Comte-Bellot, G. and Mathieu, J. (eds.), *Proceedings of the First European Turbulence Conference*, Lyon, France. Springer-Verlag, Berlin (1987) pp. 320–336.
10. Gieseke, T.J. and Guezennec, Y.G., Stochastic estimation of multipoint conditional averages and their spatio-temporal evolution. *Appl. Sci. Res.* **53** (1994) 305–320.
11. List, E.J., Turbulent jets and plumes. *Ann. Rev. Fluid Mech.* **14** (1982) 189–212.
12. Michalke, A., Instabilität eines renden Freistrahls unter Berücksichtigung des Einflusses der Strahlgrenzschichtdicke. *Z. Flugwiss.* **19** (1971) 319–328. [English translation: Instability of compressible circular free jet with consideration of the influence of the jet boundary layer thickness. NASA Tech. Memo No. 75190 (1977).]
13. Mungal, M.G. and Hollingsworth, D.K., Organized motion in a very high Reynolds number jet. *Phys. Fluids A* **1** (1989) 1615–1623.
14. Prasad, A.K. and Gonuguntla, P.V., Turbulence measurements in non-penetrative thermal convection. *Phys. Fluids* **8** (1996) 2460–2470.
15. Robinson, S.K., Kline, S.J. and Spalart, P.R., Quasi-coherent structures in the turbulent boundary layer. Part II: verification and new information from a numerically simulated flat-plate boundary layer. In: Kline, S.J. and Afgan, N.H. (eds.), *Near Wall Turbulence. Proceedings of Zaric Memorial Conference*. Hemisphere, New York (1989) pp. 218–247.
16. Siddhartha, S.S., Narasimha, R., Basu, A.J. and Kailas, S.V., Coherent structures in numerically simulated jets with and without off-source heating. *Fluid Dyn. Res.* **26** (2000) 105–117.
17. Tso, J. and Hussain, F., Organized motions in a fully developed turbulent axisymmetric jet. *J. Fluid Mech.* **203** (1989) 425–448.
18. Tso, J., Kovasznay, L.S.G. and Hussain, A.K.M.F., Search for large-scale coherent structures in the nearly self-preserving region of a turbulent axisymmetric jet. *J. Fluids Engrg.* **103** (1981) 503–508.
19. Yoda, M., Hesselink, L. and Mungal, M.G., The evolution and structure of the large-scale structures in the turbulent jet. *Phys. Fluids A* **4** (1992) 803–811.
20. Yoda, M., Hesselink, L. and Mungal, M.G., Instantaneous three-dimensional concentration measurements in the self-similar region of a round high-Schmidt-number jet. *J. Fluid Mech.* **279** (1994) 313–350.